Appendix B Structural Analysis Derivations

B.1. Introduction

Detailed derivations of selected structure analyses as introduced in Chapter Eight are compiled and presented in the following sections. The sections outline the procedures used to determine the internal actions for the nose assembly and the trunnion, both of which involve statically-indeterminate structures, as well as stress calculation for thin-walled circular tubes. These items involve derivations of the basic equations that cannot be presented in a concise manner within the main text.

B.2. The Nose Assembly

The reactions at the supports of the truss that represents the nose gear cylinder/drag/side struts structure, and consequently the internal actions, can be determined by Castigliano's theorem [46, p. 611], that is,

$$u_j = \frac{\partial U}{\partial P_j} = \sum_{i=1}^{n} \frac{F_i l_i}{A_i E} \frac{\partial F_i}{\partial P_j} \tag{B.1}$$

where u_j is the deflection at the point of application of the load P_j, E is the modulus of elasticity, and l, F, and A are the length, internal force, and cross-sectional area of each member, respectively. The above theorem gives the generalized displacement corresponding to the redundant, P_j, which is set equal to a value compatible with the support condition. This permits the solution of the redundant, and consequently all remaining internal actions, via equilibrium.

As shown in Figure B.1, the port side strut* is designated as redundant and released from its support at point *K*. Using Eq. (B.1) the deflection at point *K* can be written as

$$y_K = \frac{F_{IO} l_{IO}}{A_{IO} E} \frac{\partial F_{IO}}{\partial R_K} + \frac{F_{JO} l_{JO}}{A_{JO} E} \frac{\partial F_{JO}}{\partial R_K} + \frac{F_{KO} l_{KO}}{A_{KO} E} \frac{\partial F_{KO}}{\partial R_K} \tag{B.2}$$

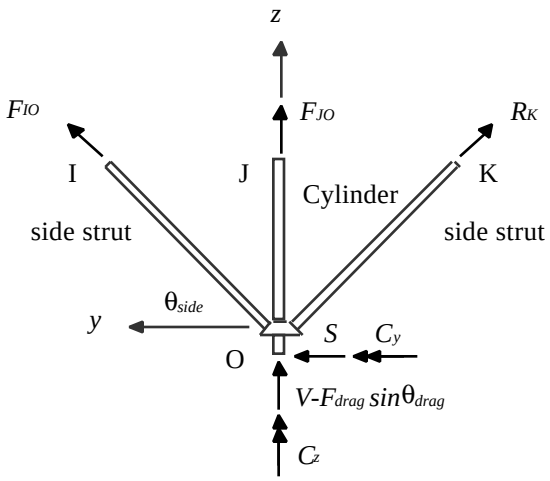

Figure B.1 Free-body diagram of the nose gear structure in the *yz*-plane

From equilibrium,

$$F_{IO} = R_K + \frac{S}{\cos\theta_{side}} \tag{B.3a}$$

$$F_{JO} = V - F_{drag} \sin\theta_{drag} - (F_{IO} + R_K)\sin\theta_{side} \tag{B.3b}$$

$$F_{KO} = R_K \tag{B.3c}$$

---

* This is the strut on the right. You are looking aft in this figure.

where S and V are the applied side and vertical force, respectively, and θ_{drag} and θ_{side} are the angles between the axial centerlines of the drag and side struts[**] and the xy-plane, respectively. Differentiating Eqs (B.3a, b, and c) with respect to R_K results in

$$\frac{\partial F_{IO}}{\partial R_K} = 1 \tag{B.4a}$$

$$\frac{\partial F_{JO}}{\partial R_K} = -sin\theta_{side} \tag{B.4b}$$

$$\frac{\partial F_{KO}}{\partial R_K} = 1 \tag{B.4c}$$

To determine the reaction at point K and subsequently the internal force in each structural component, substitute the relationships of Eqs (B.3a, b, and c) and (B.4a, b, and c) back into Eq. (B.2), apply the no-deflection condition and then solve for R_K.

B.3. The Trunnion

The trunnion model shown in Figure 8.9 is repeated here as Figure B.2. As shown in Figure B.2, the trunnion is subjected to a force with components F_x, F_y, and F_z, and a couple with moment components C_y and C_z, at axial position $x = l_1$, where $0 < l_1 < L$ and $0 \le x \le L$. Clamped end-conditions at $x = 0$ and $x = L$ yield ten homogeneous conditions, five at each end. At the load point $x = l_1$, there are five continuity conditions, *i.e.*, u, v, w, v', and w', and five jump conditions corresponding point-wise equilibrium of the internal actions and the external loads. These twenty conditions are

$$u_1(0) = u_2(L) = 0 \tag{B.5a}$$

$$v_1(0) = v_1'(0) = v_2(L) = v_2'(L) = 0 \tag{B.5b}$$

[**] A slight elaboration: the θ_{drag} is the angle between the drag strut and the x-y plane. It, along with the drag strut, is not shown in Fig. B-1 because the attachment location of the drag strut is below the side strut attachment and the figure only represents the structural arrangement at a distance above that point.

$$w_1(0) = w_1'(0) = w_2(L) = w_2'(L) = 0 \tag{B.5c}$$

$$u_1(l_1) = u_2(l_1) \tag{B.6a}$$

$$v_1(l_1) = v_2(l_1) \tag{B.6b}$$

$$w_1(l_1) = w_2(l_1) \tag{B.6c}$$

$$\frac{dv_1(l_1)}{dx} = \frac{dv_2(l_1)}{dx} \tag{B.6d}$$

$$\frac{dw_1(l_1)}{dx} = \frac{dw_2(l_1)}{dx} \tag{B.6e}$$

$$-N_{x1}(l_1) + N_{x2}(l_1) + F_x = 0 \tag{B.7a}$$

$$-V_{y1}(l_1) + V_{y2}(l_1) + F_y = 0 \tag{B.7b}$$

$$-V_{z1}(l_1) + V_{z2}(l_1) + F_z = 0 \tag{B.7c}$$

$$-M_{z1}(l_1) + M_{z2}(l_1) + C_z = 0 \tag{B.7d}$$

$$-M_{y1}(l_1) + M_{y2}(l_1) + C_y = 0 \tag{B.7e}$$

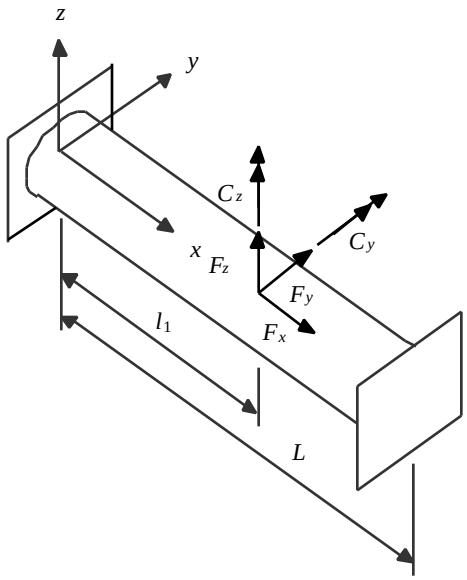

Figure B.2 Trunnion modeled as a clamped-clamped end bar

In the *xz*-plane, equilibrium gives

$$\frac{dM_y}{dx} - V_z = 0 \tag{B.8}$$

and

$$\frac{dV_z}{dx} = 0 \tag{B.9}$$

where M_y and V_z are the internal moment and shear components, respectively. Given the equation of elastic curve as

$$M_y = EI_{yy}\left(-\frac{d^2w}{dx^2}\right) \tag{B.10}$$

where E is the modulus of elasticity and I_{yy} is the second area moment about the *y*-axis, Eqs (B.8) and (B.9) become

$$V_z = EI_{yy}\left(-\frac{d^3w}{dx^3}\right) \tag{B.11}$$

and

$$EI_{yy}\left(-\frac{d^4w}{dx^4}\right) = 0 \tag{B.12}$$

Integrating Eq. (B.12) four times with respect to x results in

$$w_1 = \frac{c_1}{6}x^3 + \frac{c_2}{2}x^2 + c_3x + c_4 \qquad 0 \le x \le l_1 \tag{B.13a}$$

$$w_2 = \frac{c_5}{6}x^3 + \frac{c_6}{2}x^2 + c_7x + c_8 \qquad l_1 \le x \le L \tag{B.13b}$$

To determine w_1 and w_2 at either end of the trunnion, boundary conditions as given in Eqs (B.5b and c) and (B.6b, c, d, and e) were used to solve for the eight integration constants (c_i) in Eqs (B.13a and b). Finally, substitute w_1 and w_2 back into Eqs (B.10) and (B.11) and use the static boundary conditions as given in Eqs (B.7a, b, c, and d) to obtain the

internal shear force and bending moment, respectively. The same procedure is used to determine $v(x)$ and the internal actions in the xy-plane.

In the longitudinal direction, equilibrium gives

$$\frac{dN}{dx} = 0 \tag{B.14}$$

where N is the axial force. In addition, the material law gives

$$N = EA\frac{du}{dx} \tag{B.15}$$

where A is the cross-sectional area. Since the axial force is spatially uniform, or piecewise constant, integrating Eq. (B.15) once with respect to x results in

$$u_1 = \frac{N_1}{EA}x + c_9 \qquad 0 \le x \le l_1 \tag{B.16a}$$

$$u_2 = \frac{N_2}{EA}x + c_{10} \qquad l_1 \le x \le L \tag{B.16b}$$

where the two integration constants c_9 and c_{10} are determined using the boundary conditions as given in Eq. (B.6a). Finally, substitute u_1 and u_2 back into Eq. (B.15) and sum the forces in the x direction at $x = l_1$ to obtain the internal axial force.

B.4. Normal and Shear Stresses In a Thin-walled Tube

The normal stresses induced on the structural members are determined by combining the effects of axial load and combined bending, while the shear stresses are determined by combining the effects of torsion and shear forces due to bending [47].

The normal stress (τ_{xx},) due to combined axial force and bending moments is given as

$$\tau_{xx} = \frac{N}{A} + \frac{M_y}{I_{yy}}z - \frac{M_z}{I_{zz}}y \tag{B.17}$$

For a thin-walled circular tube referred to polar coordinates as shown in Figure B.3, the principal centroidal second area moments about the *y*- and *z*-axes are

$$I_{yy} = I_{zz} = \oint (r\sin\theta)^2 t r d\theta = \pi r^3 t \tag{B.18}$$

where r is the mean radius and t is the wall thickness. Given the relationship of Eq. (B.18), Eq. (B.17) becomes

$$\tau_{xx} = \frac{N}{A} + \frac{1}{\pi r^2 t}\left(M_y \sin\theta - M_z \cos\theta\right) \tag{B.19}$$

Differentiate Eq. (B.19) with respect to θ to get

$$\frac{d\tau_{xx}}{d\theta} = \frac{1}{\pi r^2 t}\left(M_y \cos\theta + M_z \sin\theta\right) \tag{B.20}$$

and at the extremum, *i.e.*, $d\tau_{xx}/d\theta = 0$, so that

$$\tan\theta_{max} = -\frac{M_y}{M_z} \tag{B.21a}$$

$$\sin\theta_{max} = \frac{M_z}{\sqrt{M_y^2 + M_z^2}} \tag{B.21b}$$

$$\cos\theta_{max} = -\frac{M_y}{\sqrt{M_y^2 + M_z^2}} \tag{B.21c}$$

Given the relationships of Eqs (B.21b and c), the extremum values of the bending normal stresses are determined using the expressions

$$\tau_{xx,bending}(\theta_{max}) = -\frac{1}{\pi r^2 t}\sqrt{M_y^2 + M_z^2} \tag{B.22a}$$

and

$$\tau_{xx,bending}(\theta_{max} + \pi) = \frac{1}{\pi r^2 t}\sqrt{M_y^2 + M_z^2} \tag{B.22b}$$

Thus, the extremum values of the normal stress on a circular-tube cross section under combined axial and bending actions are

$$\tau_{xx_{\substack{max \\ or \\ min}}} = \frac{N}{A} \pm \frac{1}{\pi r^2 t}\sqrt{M_y^2 + M_z^2} \tag{B.23}$$

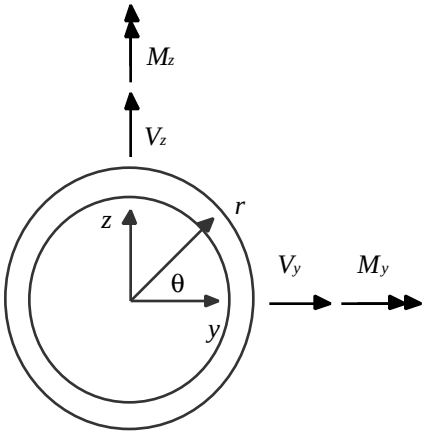

Figure B.3 Annular section showing positive shear forces and bending moments

The shear stress (τ_{xs},) due to combined transverse shear force and torque is given as

$$\tau_{xs} = \frac{q(s)}{t} + (\tau_{xs})_{torque} \tag{B.24}$$

where q is the shear flow due to bending. As indicated by in Figure B.4, the shear flow from some arbitrary origin to any point round the cross-section of a circular tube for axial equilibrium is

$$q = q_0 - \frac{dF}{dx} \tag{B.25}$$

where

$$\frac{dF}{dx} = \frac{d}{dx}\int_0^s \tau_{xx} t ds = \int_0^\theta \frac{d\tau_{xx}}{dx} t r d\theta \tag{B.26}$$

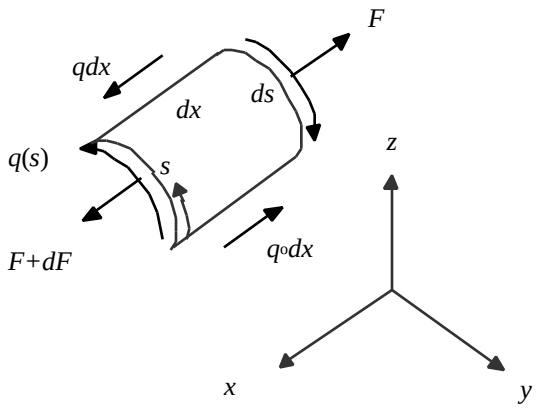

Figure B.4 Shear flow around a closed tube

Given that

$$\frac{dN}{dx} = 0 \tag{B.27}$$

$$\frac{dM_y}{dx} = V_z \tag{B.28}$$

and

$$\frac{dMz}{dx} = -V_y \tag{B.29}$$

rearrangement of Eq. (B.26) results in

$$\frac{dF}{dx} = r^2 t\left[\frac{V_z}{I_{yy}}(1-\cos\theta)+\frac{V_y}{I_{zz}}\sin\theta\right] \tag{B.30}$$

From the relationships of Eqs (B.25) and (B.30), the integral of q round the cross section is

$$\oint qrds = \oint q_0 rds - \oint \frac{dF}{dx} rds \tag{B.31}$$

Since only bending is considered in this case, the left-hand side of Eq. (B.31) is zero, that is,

$$q_0 \oint d\theta = \oint \frac{dF}{dx} d\theta \tag{B.32}$$

and the integration results in

$$q_0 = r^2 t \frac{V_z}{I_{yy}} \tag{B.33}$$

Given the relationships of Eqs (B.18), (B.30) and (B.33), the magnitude of the shear flow is determined using the expression

$$q = \frac{1}{\pi r}\left(V_z \cos\theta - V_y \sin\theta\right) \tag{B.34}$$

Differentiating Eq. (B.34) with respect to θ gives

$$\frac{dq}{d\theta} = -\frac{1}{\pi r}\left(V_y \cos\theta + V_z \sin\theta\right) \tag{B.35}$$

and at the extremum, *i.e.*, $dq/d\theta = 0$, so that

$$\tan\theta_{max} = -\frac{V_y}{V_z} \tag{B.36a}$$

$$\sin\theta_{max} = \frac{V_z}{\sqrt{V_y^2 + V_z^2}} \tag{B.36b}$$

$$\cos\theta_{max} = -\frac{V_y}{\sqrt{V_y^2 + V_z^2}} \tag{B.36c}$$

Given the relationships of Eqs (B.36b and c), the minimum and maximum values of the shear flow are determined using the expressions

$$q\left(\theta_{max}\right) = -\frac{1}{\pi r t}\sqrt{V_y^2 + V_z^2} \tag{B.37a}$$

and

$$q\left(\theta_{max} + \pi\right) = \frac{1}{\pi r t}\sqrt{V_y^2 + V_z^2} \tag{B.37b}$$

The shear stress due to torque is given as

$$(\tau_{xs})_{torque} = \frac{Tr}{J} \tag{B.38}$$

where J is the polar area moment

$$J = \int r^3 t d\theta = 2\pi r^3 t \tag{B.39}$$

So, for the thin-wall approximation the maximum stresses will occur on the contour of the circular tube, consistent with bending analysis. Thus, given the relationships of Eqs (B.37a and b) and (B.39), Eq. (B.24) becomes

$$\tau_{xs} = \frac{1}{\pi r t}\left(\frac{T}{2r} \pm \sqrt{V_y^2 + V_z^2}\right) \tag{B.40}$$